 MCB, vol.2, no.4, pp.161-177, 2005

Forced Dissociation of Selectin-ligand Complexes Using Steered Molecular Dynamics Simulation

Shouqin Lü [1] **and Mian Long**[1, 2]

Abstract: Selectin-ligand interactions are crucial to such biological processes as inflammatory cascade or tumor metastasis. How transient formation and dissociation of selectin-ligand bonds in blood flow are coupled to molecular conformation at atomic level, however, has not been well understood. In this study, steered molecular dynamics (SMD) simulations were used to elucidate the intramolecular and intermolecular conformational evolutions involved in forced dissociation of three selectin-ligand systems: the construct consisting of P-selectin lectin (Lec) and epidermal growth factor (EGF)-like domains (P-LE) interacting with synthesized sulfoglycopeptide or SGP-3, P-LE with sialyl Lewis X (sLe^X), and E-LE with sLe^X. SMD simulations were based on newly built-up force field parameters including carbohydrate units and sulfated tyrosine(s) using an analogy approach. The simulations demonstrated that the complex dissociation was coupled to the molecular extension. While the intramolecular unraveling in P-LE-SGP-3 system mainly resulted from the destroy of the two anti-parallel β sheets of EGF domain and the breakage of hydrogen-bond cluster at the Lec-EGF interface, the intermolecular dissociation was mainly determined by separation of fucose (FUC) from Ca^{2+} ion in all three systems. Conformational changes during forced dissociations depended on pulling velocities and forces, as well as on how the force was applied. This work provides an insight into better understanding of conformational changes and adhesive functionality of selectin-ligand interactions under external forces.

keyword: Force field, Separation, Extension, Applied force

[1] National Microgravity Laboratory, Institute of Mechanics, Chinese Academy of Sciences, Beijing 100080, P. R. China

[2] Corresponding author, Tel. +86-10-6261-3540. Fax. +86-10-6261-3540. E-mail: mlong@imech.ac.cn

1 Introduction

Selectin-ligand interactions play a key role for modulating tethering and rolling of circulating cells on vascular surface, a prerequisite for inflammatory cascade or tumor metastases [Springer. (1990); Springer. (1994); Vestweber and Blanks. (1999); McEver. (2001); McEver. (2002); Lawrence and Springer. (1991)]. Selectins, as a family of adhesion molecules, have three known members, P-, E-, and L-selectin. Their common structure includes an N-terminal, calcium-type lectin (Lec) domain, an epidermal growth factor (EGF)-like domain, followed by multiple copies of consensus repeat (CR) units characteristic of complement binding proteins, a transmembrane segment, and a short cytoplasmic domain. P-selectin is expressed on activated endothelial cells and platelets, E-selectin is expressed on activated endothelial cells, and L-selectin is constitutively expressed on leukocytes [Ley et al. (1991); Ushiyama et al. (1993); Kansas. (1996)]. Selectin interacts with P-selectin glycoprotein ligand 1 (PSGL-1), which is expressed on leukocytes, as well as with other carbohydrate ligands (i.e., sialyl Lewis X or sLe^X) [Moore et al. (1992); Li et al. (1996); Kansas. (1996)]. Since both selectin and PSGL-1 are well-characterized biochemically, they provide an ideal system for investigating the biophysical aspects of kinetics and mechanics of selectin-ligand interactions.

Selectin-ligand interactions are modulated by external forces. Under physiological condition, selectin interacts with PSGL-1 in two-dimension since both molecules are anchored on the surfaces of two apposing cells. This results in that their interactions are tightly coupled with mechanical environment of blood flow, which translates into an external force for modulating the dissociation of selectin-PSGL-1 bond. These have been demonstrated in early studies that bond lifetime of selectin-PSGL-1 interactions is either shortened (slip bond) [Bell. (1978); Alon et al. (1995); Chen and Springer. (1999); Chen and Springer. (2001)] or prolonged (catch bond) with applied forces [Dembo et al. (1988); Marshall et al. (2003);

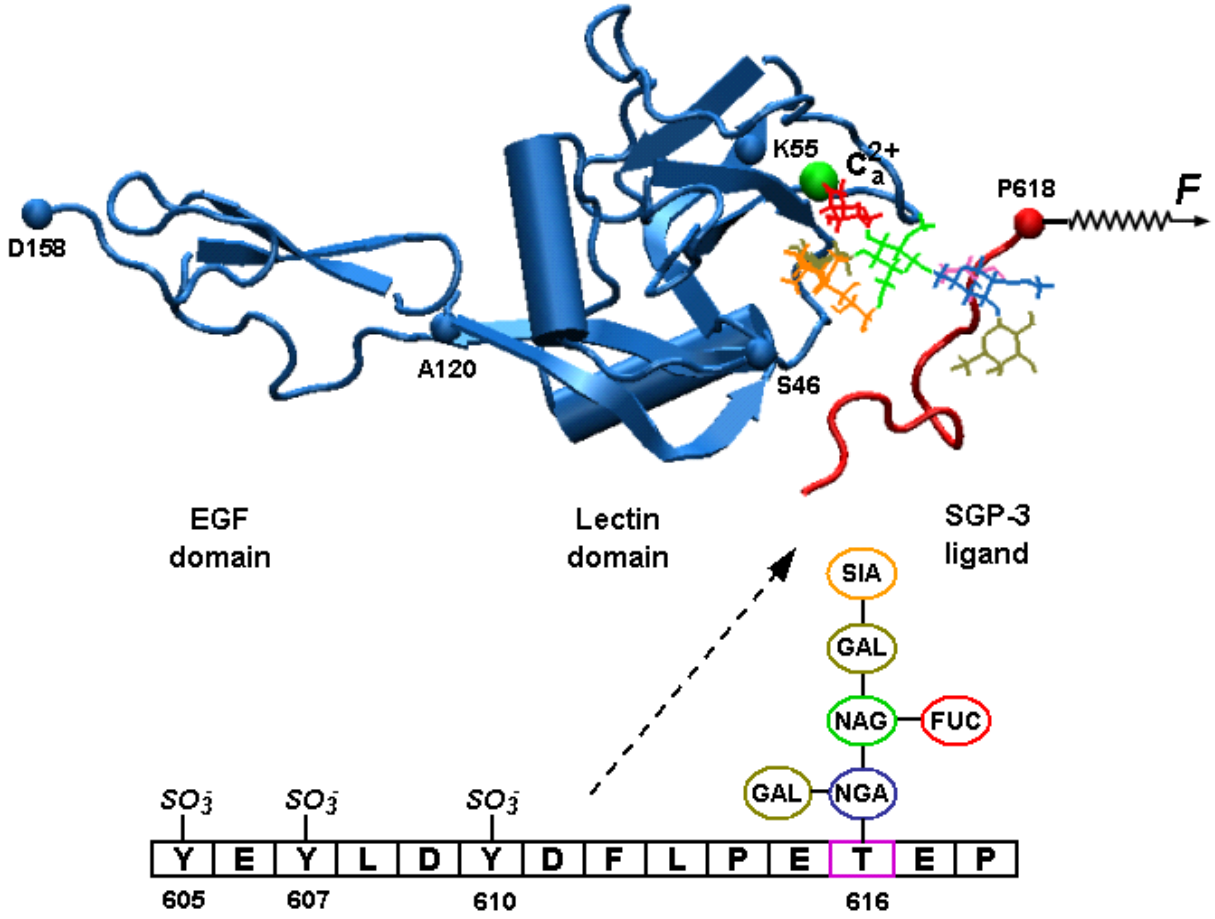

Figure 1 : Secondary structure of P-LE construct (*blue cartoon*, explicit calcium ion in *green VDW*) bound with functional PSGL-1 N terminus SGP-3 (peptide in *red cartoon*, and glycan in *resname colored lines*). Detailed components of SGP-3 were presented in lower panel. Three sets of force exertion were performed: Set I indicated the fixed end of D158-C_α of EGF C-terminal and pulled end of P618-C_α of SGP-3 peptide terminal along the force direction of D158→P618; Set II referred the fixed end of A120-C_α of Lec C-terminal and pulled end of P618-C_α along D158→P618; Set III demonstrated the alternative directions along D158→K55 or D158→S46 with the same fixed end of D158-C_α and pulled end of P618-C_α, or along the reversed direction of P618→D158 with reversed fixed and pulled ends. Other explicit presentations included all referred C_α atoms in *blue* or *red VDWs*, and force direction of D158→P618.

Sarangapani et al. (2004)], and that bond rupture force increases with loading rate of applied forces [Evans et al. (2001); Evans et al. (2004); Fritz et al. (1998); Rinko et al. (2004); Hanley et al. (2003); Zhang et al. (2004); Marshall et al. (2005b)]. To mediate leukocyte rolling in blood stream, dissociation of selectin-PSGL-1 bond in the rear should balance with bond formation in the front. This turns out to stretch the bond complex in the rear until it breaks up. Such a dynamic process suggests that the molecular extension might be coupled with the complex dissociation of selectin-PSGL-1 bond under applied forces. The underlying mechanism, however, has not been understood at an atomic level.

Selectin interacts with PSGL-1 by forming a binding pocket containing Lec-EGF (LE) domains of selectin and specific sulfoglycopeptide of PSGL-1. This is exemplified as a X-ray crystallographic structure of P-LE-SGP-3 complex [Somers et al. (2000); *cf.* Fig. 1], where SGP-3 is a synthesized sulfoglycopeptide including three potential tyrosine sulfate residues Y605, Y607, Y610, and a sLe^X-modified glycan at T616. SGP-3 is identical to 19 N-terminal amino acids of mature PSGL-1, which be-

Table 1 : Hydrogen bond occurrence and distance evolution in X-ray and MD structures.

Hydrogen bond occurrence in the X-ray and MD structures				
Atom identity		Occurrence in X-ray[¶]	Occurrence in MD equilibration	
SGP-3	P-LE		*Analogy Set*	*Optimization Set*
Y610: O2	HH11: R85	+	92.5	30.2
Y607: O1	HN: S46	-	33.6	4.4
Y607: O2	HE2: H114	+	36.5	23.3
Y607: O3	HN: S47	+	34.9	20.4
Y607: O3	HG1: S47	+	50.6	19.2
Y607: O3	HN: S46	+	17.3	10.7
Y607: O	HN: K112	+	2.0	32.7
Y605: O1/O2/O3	HZ: K112	*	67.6	17.9
SIA620: O1B	HH: Y48	+	97.8	93.4
SIA620: HO4	OG: S99	+	19.8	11.9
GAL621: HO6	OE2: E92	+	100	100
GAL621: HO4	OH: Y94	+	70.4	34.9
NAG622: O7	HE/HH22:R85	+	91.2	77.3
FUC623: HO4	OE2: E80	+	100	99.7
FUC623: O4	HD21: N82	+	94.6	93.7
FUC623: HO2	OE2: E88	+	100	100
FUC623: O3	HD21: N105	+	99.7	96.5
FUC623: HO3	OE2: E107	+	78.6	11.9
Distance evolution in X-ray and MD structures				
Atom identity		Distance in X-ray	Distance in MD equilibration	
SGP-3	P-LE		Analogy Set	Optimization Set
FUC623: O3	Ca^{2+}	2.51	2.47 ± 0.12	2.47 ± 0.15
FUC623: O4	Ca^{2+}	2.76	2.78 ± 0.31	2.88 ± 0.44

[¶]Hydrogen bonds are referred as those with a distance of donor-receptor atoms of < 4.0 Å and an interatomic angle $\geq 120^o$ in the presence (+) and absence (-) in X-ray crystal structure.
* Three oxygen atoms of SO_3^- of sulfated Y605, which are invisible in X-ray crystal structure of 1G1S, were included in SMD simulations.

haves as the smallest functional unit with as high binding affinity as wild type PSGL-1 molecule [Leppänen et al. (1999)]. The well-matched structure with a combination of electrostatic and hydrophobic contacts at the interaction interface determines the high binding affinity of selectin-PSGL-1 interactions. There are two major binding epitopes: one is the interaction of sLe^X-modified glycan with P-LE mainly by fucose unit (FUC) interacting with Ca^{2+} ion and its nearby residues, and another is the interaction of three sulfated tyrosines (Y605, Y607, and Y610) with P-LE by hydrogen bonds (H-bonds) or water bridges [Somers et al. (2000); *cf.* Table 1]. Early studies demonstrated that at least one sulfated tyrosine is required for molecular recognition [Ramachandran et al. (1999)], and de-glycosylation abrogates the binding of PSGL-1 to selectin [Leppänen et al. (2003)]. Therefore, it is of great interests in understanding what kind of roles of these specific interactions play during forced dissociation of selectin-PSGL-1 interactions.

Steered molecular dynamics (SMD) simulation is a well-developed approach to conduct the simulations of force-induced molecule unfolding and complex dissociation by introducing external forces into molecular dynamics simulations [Isralewitz et al. (2001)], which can provide the time-dependent conformational changes at atomic level on the time scale accessible to molecular dynamic simulations. SMD simulations have been widely used in studying the mechanism of forced protein unfolding [Lu et al. (1998); Gao et al. (2002)]. It has also been used

to investigate the structural information and structure-function relationship of unbinding of biomolecular complex under applied forces [Izrailev et al. (1997); Bayas et al. (2003); Bayas et al. (2004)]. The validity of this approach has been confirmed by correlating qualitatively the simulations with experimental data [Marszalek et al. (1999)] or interpreting successfully the experimental observations [Merkel et al. (1999)]. In this study, SMD simulations were used to study the mechanism of forced dissociation of three selectin-ligand systems: P-LE-SGP-3, P-LE-sLe^X, and E-LE-sLe^X. A new force field including carbohydrate units and/or sulfated tyrosine was developed to perform the SMD simulations for selectin-ligand complexes. Detailed conformational changes and specific interactions were obtained under constant velocities and forces, which provide new insights into how external force regulates the dissociation of selectin-ligand complex.

2 Methods

2.1 Force field development

Selectin ligands contain glycosylated units and/or sulfated tyrosine(s). For example, SGP-3 has two epitopes required for molecular recognition: a core 2-branched O-glycan (C2-O-sLe^X) at T616 and three sulfated tyrosine (TYS) residues Y605, Y607, and Y610 (Fig. 1) [Somers et al. (2000)]. C2-O-sLe^X contains six units: two β-D-galactoses (β-D-GAL), a N-acetyl-D-glucosamine (β-D-NAG), a N-acetyl-D-galactosamine (α-D-NGA), a α-L-fucose (α-L-FUC), and a α-L-sialic acid (α-L-SIA). Unfortunately, the lack of force field parameters of these two important components makes the molecular dynamic simulations impossible. Based on existing CHARMM22 force field parameters [MacKerell et al. (1998)], two sets of parameters were developed for C2-O-sLe^X and TYS using analogy approach and partial optimization with *ab-initio* calculations, which were referred as *Analogy Set* and *Optimization Set* respectively.

The *Analogy Set* force field was developed using analogy and model combination approaches [Foloppe and MacKerell. (2000)]. Force field of β-D-GAL was obtained by analogy from that of α-D-glucopyranose (α-D-GLC) existed in CHARMM22 [MacKerell et al. (1998)]. These two residues served as model compounds for building other residues.Force fields of β-D-NAG and α-D-NGA were developed by model combination of their respective carbohydrate units with acetamide (ACEM), while those of α-L-FUC and α-L-SIA were established by combination of GLC and CH_3 models, and by combination of GLC, ACEM, and COO^- at amino acid residue GLU or ASP, respectively. All glycan linkages were parameterized in the same combination way. Force field of TYS was built upon combining tyrosine with SO_3^- of model dodecylsulphate (SDS) or methylsulfate (MSO_4). Partial charges of joint-atoms between any combinations were re-adjusted following the general rule of CHARMM force field construction [MacKerell et al. (1998); Foloppe and MacKerell. (2000)]. Equilibrium bond length, angles, torsional angles, and force constants of new born residues were generated from X-ray coordinates and parameters of similar chemical structure available in CHARMM22 force field [MacKerell et al. (1998)]. No any new atom types were introduced during the development.

To develop *Optimization Set* force field, *Analogy Set* force field was partially optimized on partial charges and dihedrals of joint-atoms of new residues, following the same way as CHARMM force field optimization does [MacKerell et al. (1998); Foloppe and MacKerell. (2000)]. Briefly, each residue was optimized using GAUSSIAN98 program at the Hartree-Fock level with a 6-31G* basis set [Frisch et al. (2001)]. The topology of internal coordinate in *Analogy Set* was then adjusted upon the above optimization. For partial charge optimization, the target data was the scaled *ab-initio* interaction energy by factor of 1.16 between target atom and water model TIP3P generated using GAUSSIAN98 [Frisch et al. (2001)]. The corresponding MD value obtained from CHARMM program [Brooks et al. (1983)] was iterated by adjusting partial charges of target atom and its nearby atom cluster to match such the scaled *ab-initio* value. Dihedral optimization was done, after atom partial charges in *Analogy Set* force field were replaced by the optimized charges, using the same way as the partial charge optimization does, except that the target data here was the *ab-initio* relative potential energy surface [MacKerell et al. (1998); Foloppe and MacKerell. (2000)]. Considering the coupling of force field parameters, atom partial charges were re-optimized after dihedral optimization. The force field resulted was defined as *Optimization Set* force field.

2.2 SMD simulations

SMD simulations of forced dissociation of selectin-ligand complexes were performed using the program NAMD2 [Kale et al. (1999)] with force field of CHARMM22 [MacKerell et al. (1998)] for protein and newly built-up force field for glycan and/or sulfated tyrosine, plus the program VMD [Humphrey et al. (1996)] for simulation analyses and structure visualizations. The corresponding X-ray crystal structure for P-LE-SGP-3 (deposited as entry 1G1S in Protein Data Bank or PDB [Bernstein et al. (1977)]), P-LE-sLe^X (as entry 1G1R in PDB), or E-LE-sLe^X (as entry 1G1T in PDB) complex was used as the starting point [Somers et al. (2000)].

To perform SMD simulations, monomeric P-LE-SGP-3 complex was adopted from entry 1G1S in PDB. The corresponding strontium ion Sr^{2+} was replaced by a calcium ion Ca^{2+} since P-selectin-PSGL-1 interactions were Ca^{2+}-dependent physiologically. The P-LE-SGP-3 complex was solvated in a sphere of explicit water molecules with radius of 53 Å, using the plug-in package SOLVATE of program VMD [Humphrey et al. (1996)]. Thirteen Cl^- and fifteen Na^+ ions were added for neutralizing the system. The resulted P-LE-SGP-3 system, centered in the spherical water bubble, had the complex surface covered everywhere by at least 4-5 water shells with $\sim$ 60,200 atoms totally, and 3,231 of which belong to the complex.

The simulations were performed with a time step of 1 femtosecond (*fs*), a uniform dielectric constant of 1.0, a cut-off of non-bonded interactions with a switching function starting at a distance of 11 Å and reaching zero at 14 Å, and the scaling factor for 1-4 interactions of 1.0. Before heating the system, the initial configuration was minimized for 5,000 steps (3,000 steps with fixed backbone atoms of P-LE and of peptide of SGP-3, Ca^{2+} ion, and no-hydrogen atoms of glycan, and 2,000 steps without any fixation). Then the system was heated over 25,000 steps to 300 K gradually with 30 K increments per 2,000 steps followed by an equilibration process of another 5,000 steps. During 1.6-*ns* equilibration with thermal bath of 300 K, the temperature was controlled using Langevin dynamics, and the water molecules composed of the outer 5 Å shell of the system were harmonically restrained to their positions to keep the water bubble shape with the periodic re-adjustment every 300 *ps*. Finally, 20 *ps* of free dynamics was performed with thermal bath without harmonic restraints. The resulting equilibration conformation was used for SMD simulations.

SMD simulations were performed by applying forces using both constant velocity (*cv*-SMD) and constant force (*cf*-SMD) algorithms [Isralewitz et al. (2001)], corresponding to similar procedures used in rupture force [Fritz et al. (1998); Hanley et al. (2003); Marshall et al (2005b)] and lifetime [Marshall et al. (2003); Sarangapani et al. (2004)] measurements of selectin-PSGL-1 dissociation in atomic force microscopy (AFM) assay. In *cv*-SMD simulations, time dependence of external force follows $F = k\ (vt - \Delta x)$, where Δx is the displacement of the pulled end from its original position at time t = 0, which measures the extension of the complex, v is the velocity of one end of a harmonic spring which was attached to the pulled atom by the other end [Lu et al. (1998)], and k is the spring constant which gave 100 pN/Å ($\sim 1.5 k_B T/$Å^2, corresponding to the thermal fluctuation of the constrained pulled end to $\delta x = \sqrt{(k_B T/k)} \approx$ 0.82Å).

Three sets of force exertion were used (Fig 1): Set I indicated the fixed end of D158-C_α of EGF C-terminal and pulled end of P618-C_α of SGP-3 peptide along the force direction of D158→P618, which was used for both *cv*- and *cf*-SMD simulations at constant velocity of 1.5-0.05 Å/ps or at constant force of 1500-500 pN; Set II referred the fixed end of A120-C_α of Lec C-terminal and pulled end of P618-C_α along D158→P618, which was used to perform *cv*-SMD simulations at 1.0-0.1 Å/ps; Set III demonstrated the alternative directions along D158→K55 or D158→S46 with the same fixed end of D158-C_α and pulled end of P618-C_α, or along the reversed direction of P618→D158 with the reversed fixed and pulled ends, which was used to perform *cv*-SMD simulations at 0.1 Å/ps.

SMD simulations were also performed with periodic boundary condition and full electrostatic calculations to quantify the effects of different boundary conditions and incomplete electrostatic calculations. The original coordinate system of the complex was first transformed to one where the x-axis is along the line joining the fixed end of D158-C_a and pulled end of P618-C_a, and the force was applied along the x-axis. The complex was solvated in a box of explicit water molecules with dimensions of 154.8 $\times$ 66.8 $\times$ 71.8 Å^3. After system neutralization and energy minimization as described above, the system was equilibrated at 300 K and 1 *atm* for 1.6 *ns* with a fixed D158-C_α and a restrained P618-C_α to move freely only

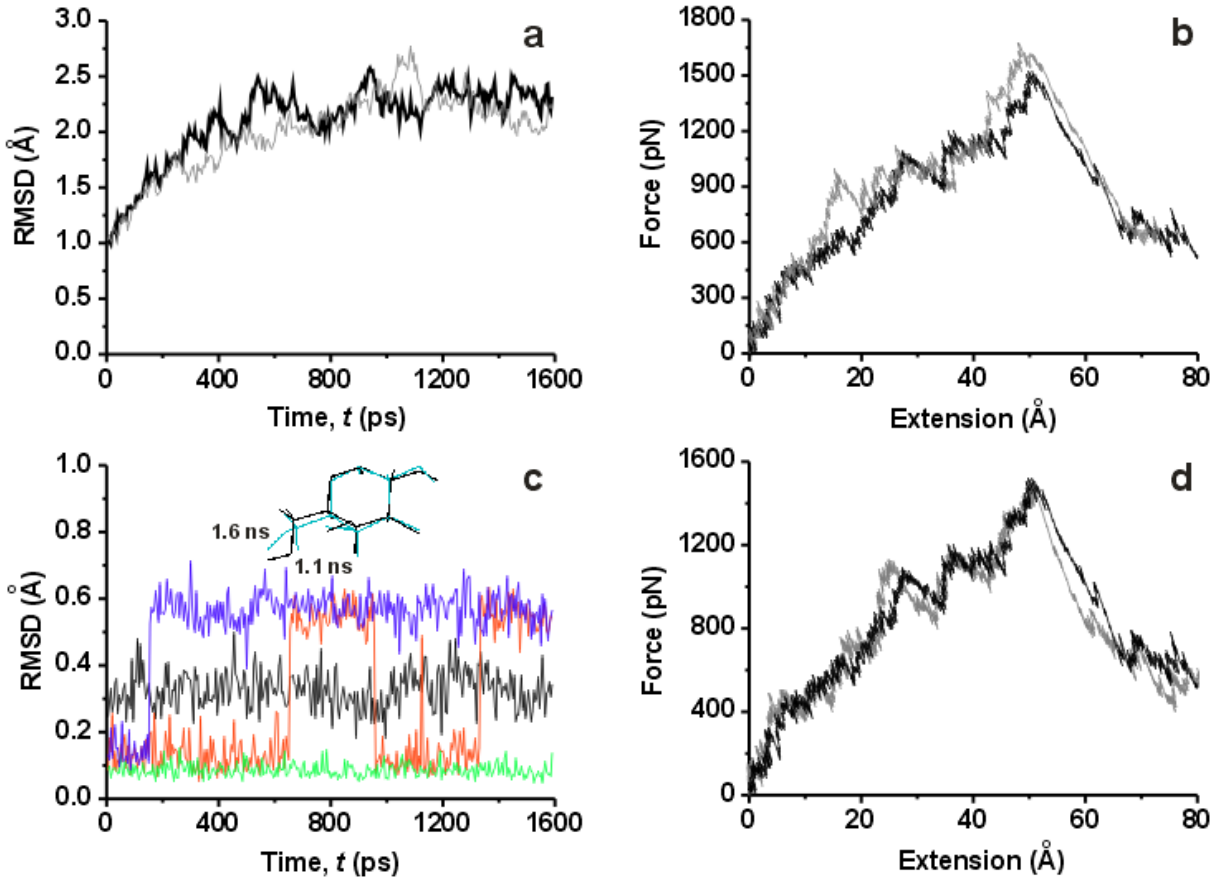

Figure 2 : Equilibration and forced dissociation dependences of P-LE-SGP-3 complex on force field parameters. (*a*) Time evolutions of all-atom RMSD during equilibration processes using force field parameters of *Analogy Set* (*black*) and *Optimization Set* (*gray*). (*b*) Force *vs.* extension profiles at 0.1Å/ps upon *Analogy Set* (*black*) and *Optimization Set* (*gray*). (*c*) Time evolutions of no-hydrogen RMSD of individual glycan residues during equilibration using parameters of *Analogy Set* (SIA620: *black*; GAL621: *red*; FUC623: *green*; GAL624: *blue*). Both GAL621 and GAL624 presented obvious conformational distortion. The *insert* showed conformational comparisons of GAL621 before (*black*) and after (*cyan*) distortion. (*d*) Force *vs.* extension profiles at 0.1Å/ps with initial conformations of 1.1-*ns* equilibration without GAL621 distortion (*gray*) and of 1.6-*ns* equilibration with GAL621 distortion (*black*).

in the *x* direction. All-atom RMSD of the complex during the last 800 *ps* of isothermal-isotonic equilibration was 2.50 $\pm$ 0.14 Å, and the size of water box at the end of equilibration was 156.1 $\times$ 64.0 $\times$ 69.3 Å^3. The final configuration after 1.6-*ns* equilibration was used as the starting point to perform SMD simulations at 0.1 Å/ps.

SMD simulations were further performed for two additional selectin-ligand complexes, P-LE-sLe^X and E-LE-sLe^X, to compare with those for P-LE-SGP-3 complex. Both complexes were built and equilibrated as spherical P-LE-SGP-3 system described above with different system sizes (radius of 48 Å and $\sim$ 44,000 atoms), diverse Cl^- and Na^+ ions for system neutralization (16 and 10 of Cl^- and 12 and 11 of Na^+ ions for P-LE-sLe^X and E-LE-sLe^X, respectively), and distinct equilibration time (1.1 *ns*). All-atom RMSD during last 500 *ps* equilibration processes was 1.27 $\pm$ 0.15 and 1.93 $\pm$ 0.15 Å for P-LE-sLe^X and E-LE-sLe^X, respectively. Upon the final configuration as the starting point, *cv*-SMD simulations were performed at 0.5 Å/ps with a fixed end of D158-C_α and pulled end of NAG903-C_1 along D158→NAG903 for P-LE-sLe^X, or with a fixed end of V157-C_α and pulled end of NAG603-C_1 along V157→NAG603 for E-LE-sLe^X.

2.3 Simulation Analyses

To determine the molecular extension, intramolecular destroy and intermolecular disruption quantitatively, several atom-atom distances were defined to measure the dissociation of selectin-ligand complex. Here Δx described above is referred as the "extension" to demonstrate the whole deformation of the complex, and the distance between geometric centers of Lec domain and its ligand along force direction was defined as the "separation" to illustrate the complex dissociation. Other definitions included the distance D1 between geometric centers of backbone atoms of two β strands, G131-E135 and Y140-C144, to evaluate the destroy of the major anti-parallel β sheets of EGF domain, and the distance D2 between C_α of T2 (S2 for E-LE) and C_α of I137 to estimate the destroy of Lec-EGF interface, and the distance D3 between Ca^{2+} ion and geometric center of FUC unit to display the beginning of intermolecular dissociation. In addition, the backbone RMSDs of Lec (W1-A120) and EGF (S121-D158 for P-LE and A121-V157 for E-LE) domains were also calculated for estimating their destroys, respectively.

3 Results

3.1 Newly built-up force field is applicable to perform SMD simulations

Both *Analogy* and *Optimization Sets* were used to perform the equilibration and SMD simulations for P-LE-SGP-3 complex. The all-atom RMSD of the complex and hydrogen bond occurrence at the interface during equilibration, and the force *vs.* extension profile during SMD simulations were used to validate the applicability of the two force fields. The RMSD evolution exhibited a transient phase and reached an equilibrium plateau, resulting in 2.33 ± 0.09 and 2.17 ± 0.12 Å upon *Analogy Set* (*black*) and *Optimization Set* (*gray*), respectively, during the last 400-*ps* equilibration (Fig. 2*a*). The hydrogen bond occurrence was defined as the fraction of that hydrogen bond occurring in the 1.6-*ns* equilibration process. Major hydrogen bonds at the interface of P-LE-SGP-3 complex and the distance between Ca^{2+} ion and oxygen atoms in FUC623 were conservative as compared to those shown in original X-ray structure (Table 1). The stability of spatial conformation and H-bonding pattern inherent at the interface provided a strong support to the proposed parameterization of force field for C2-O-sLe^X and TYS. Followed SMD simulations at 0.1 Å/ps presented the similar force *vs.* extension profiles upon both force fields (Fig. 2*b*). Although both force fields resulted in qualitative consistence during equilibration and forced dissociation, the less hydrogen bond occurrence was still found in *Optimization Set* (Table 1). Therefore, *Analogy Set* force field and corresponding system were selected for following SMD simulations.

To further test the applicability of force field, time evolution of no-hydrogen RMSD of individual glycan residues during equilibration was analyzed on *Analogy Set*. While SIA620 (*black*), FUC623 (*green*), as well as NAG622 and NGA625 conserve well their conformations, structure distortions of GAL621 (*red*) and GAL624 (*blue*) were found during equilibration, indicating the flexibility of the carbohydrate groups (Fig. 2*c*; NAG622 and NGA625 were not shown for clarity) [Kirschner and Woods. (2001); Kuttel et al. (2002)]. SMD simulations, however, demonstrated that the force *vs.* extension profile exhibited the same evolution when the starting conformation for simulations was chosen as the one at 1.1-*ns* equilibration without GAL621 distortion (*gray*) or at 1.6-*ns* equilibration with GAL621 distortion (*black*) (Fig. 2*d*), suggesting that the dissociation was insensitive to GAL distortion probably due to its less importance in adhesions. Taken together, *Analogy Set* is applicable to SMD simulations of forced dissociation of selectin-ligand interactions.

3.2 Intermolecular disruption is coupled to intramolecular destroy

cv-SMD simulation was performed to study intensively the forced dissociation of P-LE-SGP-3 complex at constant velocity of 0.1 Å/ps with fixed end of D158-C_a atom, pulled end of P618-C_a, and force direction along D158→P618 (Set I; *cf.* Fig. 1). Force increased initially at a rate of 60 pN/Å without essential rupture within the first extension of 7.7 Å (Fig. 3*a*). The rate of force increase reduced to 23.8 pN/Å at 7.7-25.8 Å, indicating the destroy of the minor anti-parallel β sheets of EGF domain (*point 2* in Fig. 3*a*). Followed was the sequential intramolecular destroy mainly on the major anti-parallel β sheets of EGF domain and Lec-EGF interface up to 45.5 Å (*point 5* in Fig. 3*a*), until which no essential intermolecular disruption occurred except of the H-bond breakage between SIA620 and Y48. The intermolecular disruption appeared when FUC623 began to dissociate

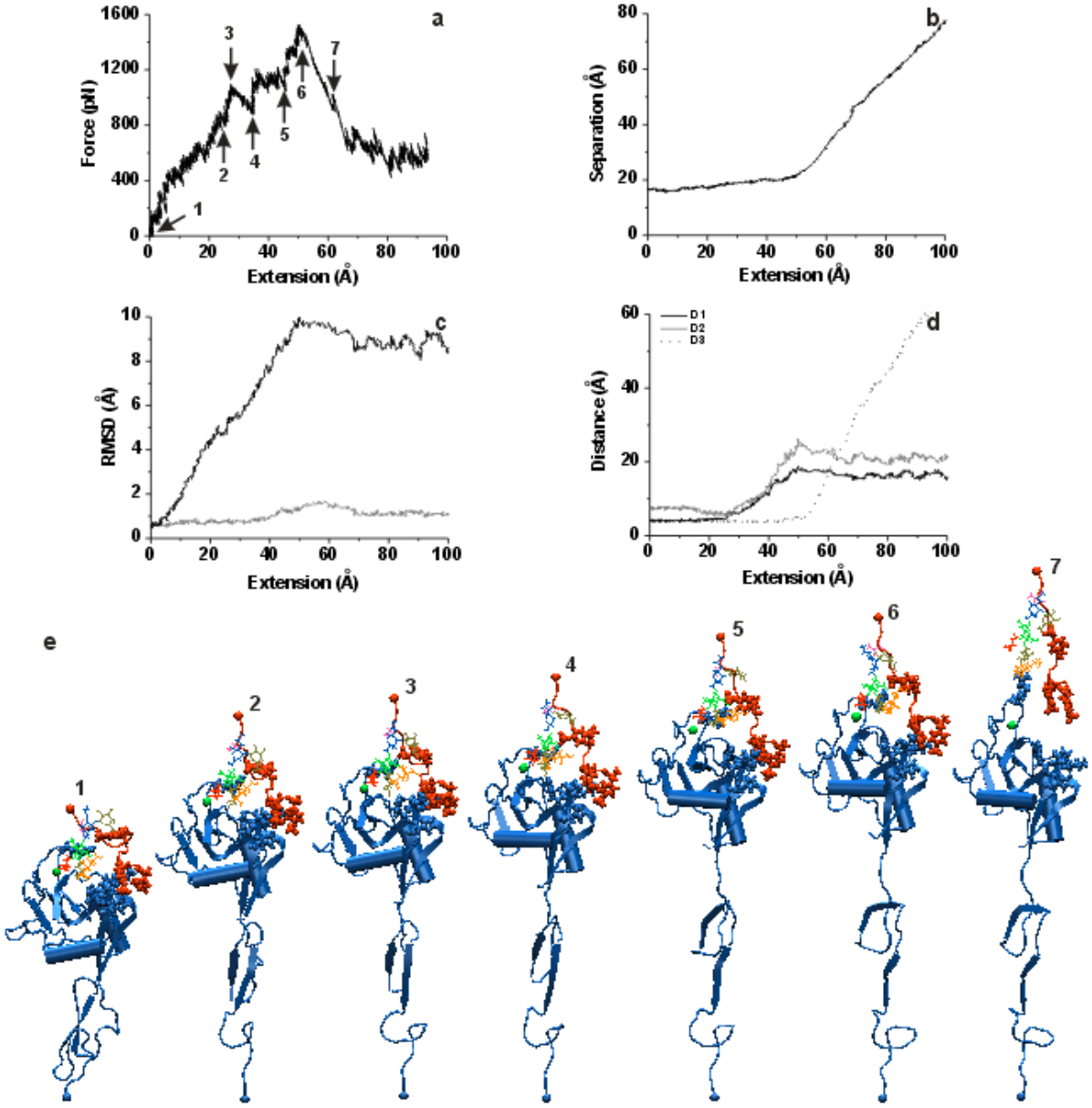

Figure 3 : Forced dissociation of P-LE-SGP-3 complex using force exertion of Set I. (*a*) A typical force *vs.* extension profile at 0.1 Å/ps. (*b*) Corresponding separation evolution with extension. (*c*) Evolutions of the backbone RMSD of Lec (*gray*) and EGF (*black*) domains. (*d*) Distance evolutions of D1 (*black solid line*), D2 (*gray solid line*), and D3 (*black dot line*). (*e*) Snapshots of the complex during dissociation. Three sulfated tyrosines of SGP-3 and their respective counterpart residues of P-LE were presented markedly in *red* and *blue VDW*, respectively.

from Ca^{2+} ion (*point 6* in Fig. 3*a*), and developed until the complex dissociated completely. Such a transition was further observed by the fact that the separation exhibited an insensitive phase when the extension increased initially and a transient phase beyond 51.5 Å (Fig. 3*b*), indicating that the molecular extension occurred prior to the complex separation. Correspondingly, the backbone RMSD of EGF domain increased initially and reached to a plateau of $\sim$ 9.6 Å (*black line* in Fig. 3*c*), and the distances of D1 and D2 began to increase from $\sim$ 25.3 Å and reached a plateau beyond 45.5 Å (*black* and *gray lines* in Fig. 3*d*), suggesting that EGF domain and Lec-EGF interface experienced significant destroys during complex dissociation. The Lec domain kept its integrity (*gray line*

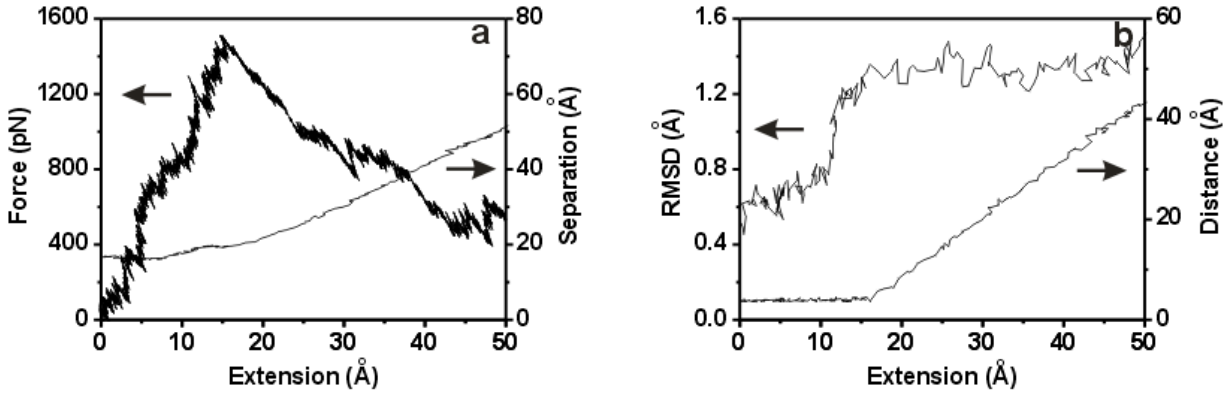

Figure 4 : Forced dissociation of P-LE-SGP-3 complex using force exertion of Set II. (*a*) Force *vs.* extension profile (*black line* and *left abscissa*) and corresponding separation evolution (*gray line* and *right abscissa*) at 0.1 Å/ps. (*b*) Evolutions of backbone RMSD of Lec domain (*black line* and *left abscissa*) and of distance D3 (*gray line* and *right abscissa*).

in Fig. 3*c*). The transient point of evolution of distance D3 (*dot line* in Fig. 3*d*) was parallel to that in the complex separation (Fig. 3*b*), implying that the complex dissociation occurred when FUC623 separated from Ca^{2+} ion.

The relationship between intramolecular destroy and intermolecular disruption was further observed by force evolution. The first force peak of $\sim$ 1000 pN at $\sim$ 27.6 Å (*point 3* in Fig. 3*a*) corresponded to destroy the major anti-parallel β sheets of EGF domain and break the H-bond cluster of Lec-EGF interface, while the second of $\sim$ 1500 pN at $\sim$ 51.5 Å (*point 6* in Fig. 3*a*) corresponded to initiate the separation of FUC623 from Ca^{2+} ion. The following rupture of H-bonds between three sulfated tyrosines and their counterpart amino acids did not exhibit obvious force peaks. Structural snapshots were exemplified in Fig. 3e to illustrate the relevant conformational variations.

Additional test was to neglect the destroy of EGF domain and Lec-EGF interface in *cv*-SMD simulations. This was done by performing the simulations at 1.0-0.1 Å/ps with fixed end of A120-C_α of Lec C-terminal and pulled end of P618-C_α along D158→P618 (Set II; *cf.* Fig. 1). Only the data at 0.1 Å/ps were shown in Fig. 4 for clarity. By comparison with the above simulations under Set I (*cf.* Fig. 3), only one force peak ($\sim$1500 pN) was found in force *vs.* extension profile (Fig. 4*a*; *left abscissa*), and the insensitive phase in separation *vs.* extension profile diminished (Fig. 4*a*; *right abscissa*). RMSD of Lec domain increased initially and then quickly jumped to reach a plateau of $\sim$ 1.3 Å at the extension of $\sim$ 16.1 Å (Fig. 4*b*; *left abscissa*), at which FUC623 began to dissociate from Ca^{2+} (Fig. 4*b*; *right abscissa*). This further validated that molecular extension was mainly due to the destroy of EGF domain and Lec-EGF interface while Lec domain kept its integrity.

3.3 *Dissociation depends on pulling velocities and forces*

To test the effect of pulling velocity, *cv*-SMD simulations for P-LE-SGP-3 complex were compared at five velocities of 1.5, 1.0, 0.5, 0.1, and 0.05 Å/ps using force exertion of Set I. For the sake of clarity, only the data at 1.5, 0.5, and 0.05 Å/ps were shown in Figs. $5a-b$. At low velocity (0.05 Å/ps), two force peaks appeared with force values of $\sim$ 1000 pN at 26.7 Å and of $\sim$ 1250 pN at 45.7 Å (*black line* in Fig. 5*a*), similar to the above force *vs.* extension profile at 0.1 Å/ps with the smaller second force peak (*cf.* Fig. 3). The intramolecular destroy of EGF domain and Lec-EGF interface was again observed, followed by the intermolecular disruption (*black line* in Fig. 5*b*). At intermediate velocity (0.5 Å/ps), the force profile exhibited a flat force peak of $\sim$ 1850 pN at 39.3 Å followed by a peak of $\sim$ 1950 pN at 46.7 Å (*gray line* in Fig. 5*a*). The separation *vs.* extension profile also demonstrated a similar insensitive phase as that at 0.05 Å/ps except slightly shifting rightwards (*gray line* in Fig. 5*b*). At high velocity (1.5 Å/ps), the first peak vanished completely and the second one of $\sim$ 2800 pN shifted leftwards at 27.7 Å. The intermolecular disruption started to happen from 26.9 Å right after destroying the minor anti-

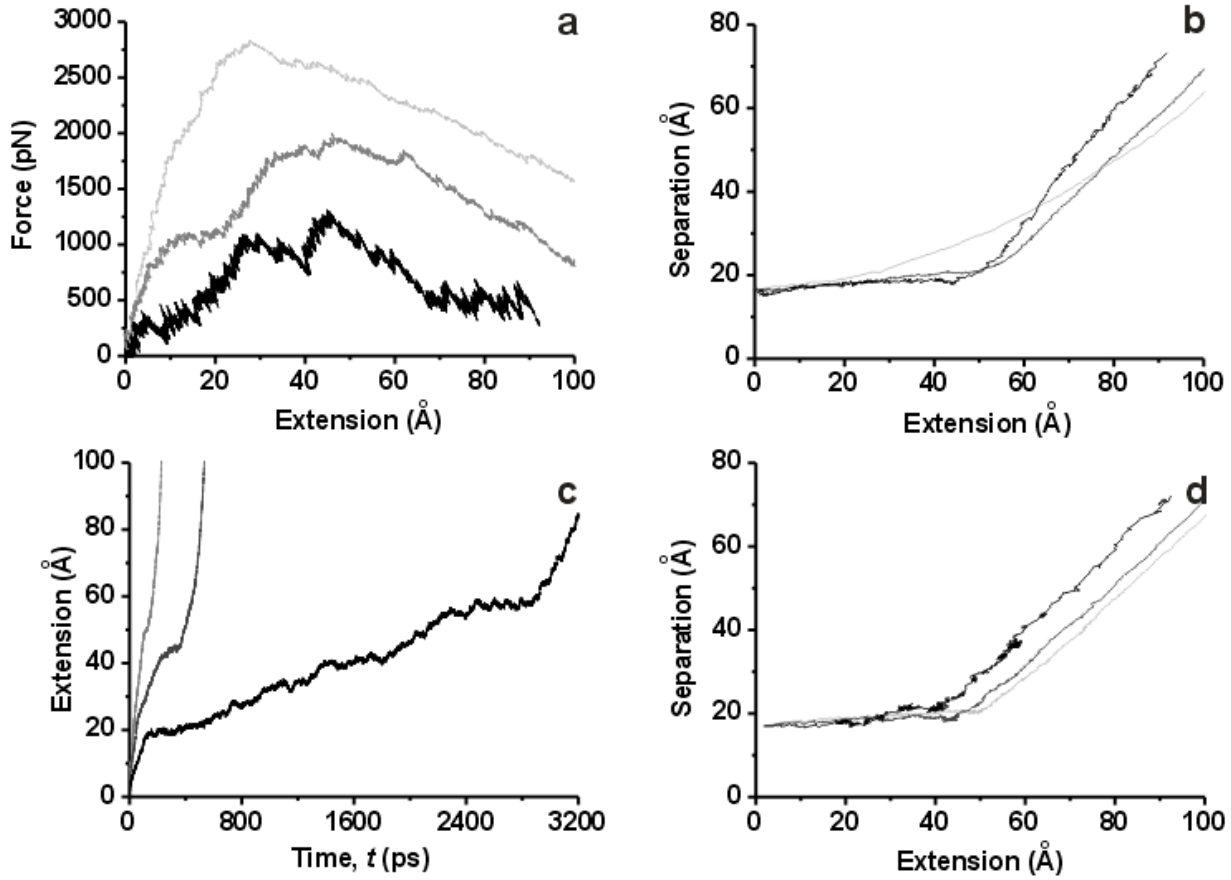

Figure 5 : Dependence of forced dissociation of P-LE-SGP-3 complex on pulling velocities and forces using force exertion of Set I. (*a*) Force *vs.* extension profiles and (*b*) corresponding separation evolutions (*light gray*: 1.5 Å/ps; *gray*: 0.5 Å/ps; *black*: 0.05 Å/ps). (*c*) Extension *vs.* time profiles and (*d*) corresponding separation evolutions (*light gray*: 1500 pN; *gray*: 1000 pN; *black*: 500 pN).

parallel β sheets of EGF domain, resulting in the disappearance of the insensitive phase of separation (*light gray lines* in Figs. $5a-b$). Even so, the intramolecular destroy still evolved further with evolution of intermolecular disruption (*light gray line* in Fig. 5*b*). It is evident that the higher the velocity was, the larger the rupture force was obtained, and the less the destroy of EGF domain and Lec-EGF interface was found before intermolecular disruption. The integrity of Lec domain was independent on pulling velocities.

Additional test was conducted to quantify the effect of constant forces on dissociations of P-LE-SGP-3 complex at 1500, 1000, and 500 pN (Fig. $5c-d$). The corresponding extension *vs.* time profiles, shown in Fig. 5*c*, exhibited a transition of both plateaus and shoulders. At low force of 500 pN, two major plateaus appeared with extension values of 19 Å at 135 *ps* and of 40 Å at 1386 *ps*, corresponding to the starting points of intramolecular destroy and intermolecular disruption, respectively. Another plateau beyond 2400 *ps* resulted from strong H-bond interactions between R85 and D611, which was formed after H-bond breakage of R85 and Y610, followed by increased separation of complex again until complete dissociation (*black line* in Fig. 5*c*). At intermediate or high force of 1000 or 1500 pN, the extension shifted leftwards significantly accompanied with vanished plateaus (*gray* and *light gray lines* in Fig. 5*c*), implying that the higher the force was applied, the shorter the bond survived. Again, the intramolecular destroy was coupled with the intermolecular disruption accompanied by the integrity of Lec domain on various forces (Fig. 5*d*).

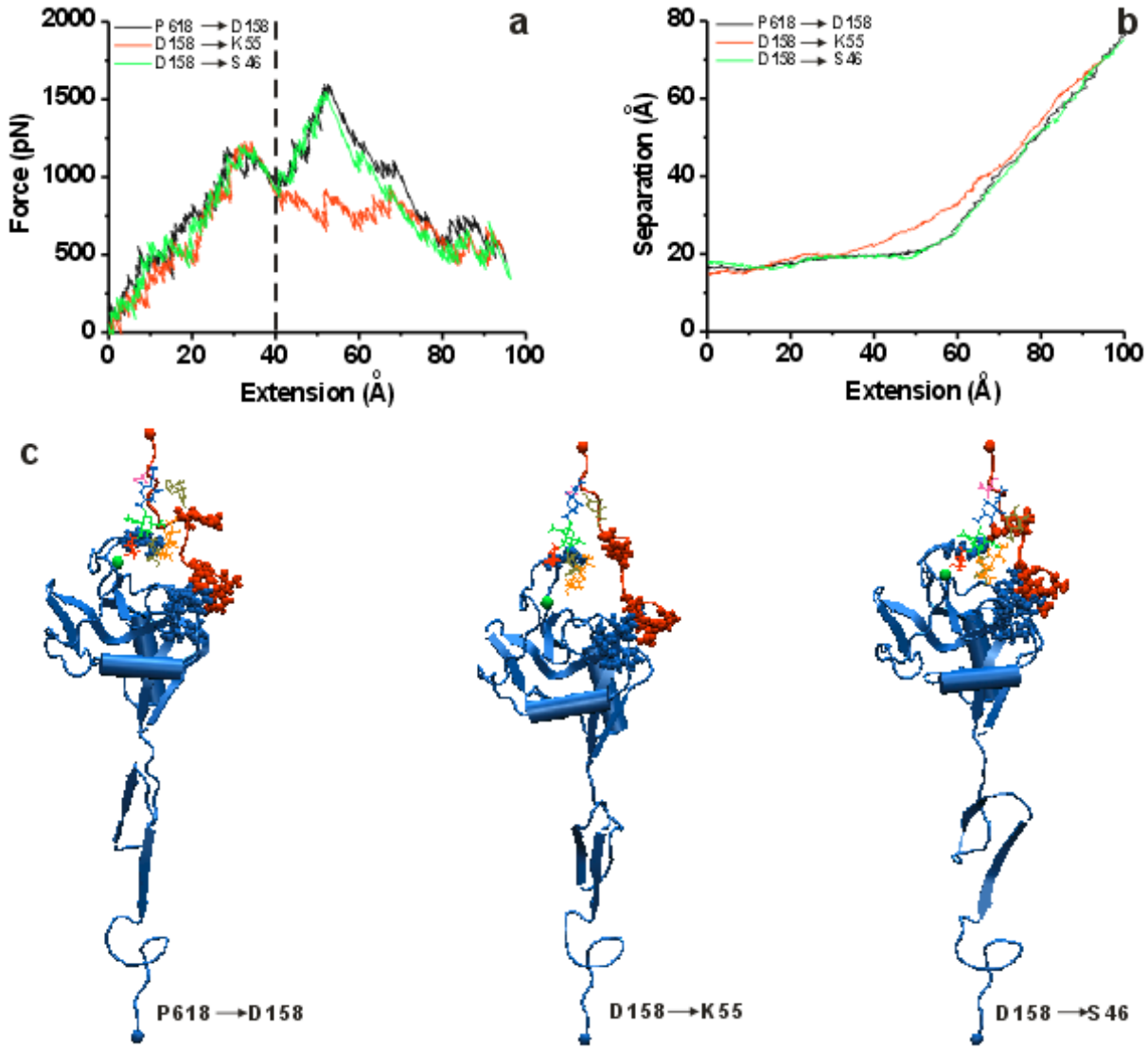

Figure 6 : Dependence of forced dissociation of P-LE-SGP-3 complex on force directions using force exertion of Set III at 0.1 Å/ps. (*a*) Force *vs.* extension profiles. (*b*) Corresponding separation evolutions. (*c*) Snapshots at the same extension of 40 Å.

3.4 Dissociation is modulated by force directions

To test the effect of force exertion, *cv*-SMD simulations were performed at 0.1 Å/ps by alternative directions along D158→K55 or D158→S46 with the same fixed end of D158-C_α and pulled end of P618-C_α, or along the reversed direction of P618→D158 with reversed fixed and pulled ends (Set III; *cf.* Fig. 1) (Fig. 6). It was found that the two force peaks still appeared and that the intramolecular destroy was coupled with the intermolecular disruption (*black and green lines* in Fig. $6a-b$) along D158→S46 or P618→D158, which were consistent with the above results along D158→P618 (*cf.* Fig. 3). The force *vs.* extension profile along D158→K55, however, exhibited an exceptional transition, that is, only one force peak appeared at 30 Å (*red line* in Fig. 6*a*). Conformational analyses demonstrated that such a transition resulted from the synchronization of the intramolecular destroy and intermolecular disruption (*red line* in Fig. 6*b*). P-LE-SGP-3 complex dissociated along D158→K55 more like sliding SGP-3 over the line from Y605 to P618 with smaller resistance, while it dissociated along D158→S46 or P618→D158 just like peeling SGP-3 off with larger resistance. This turned out to be the alternative mechanism of dissociation with different

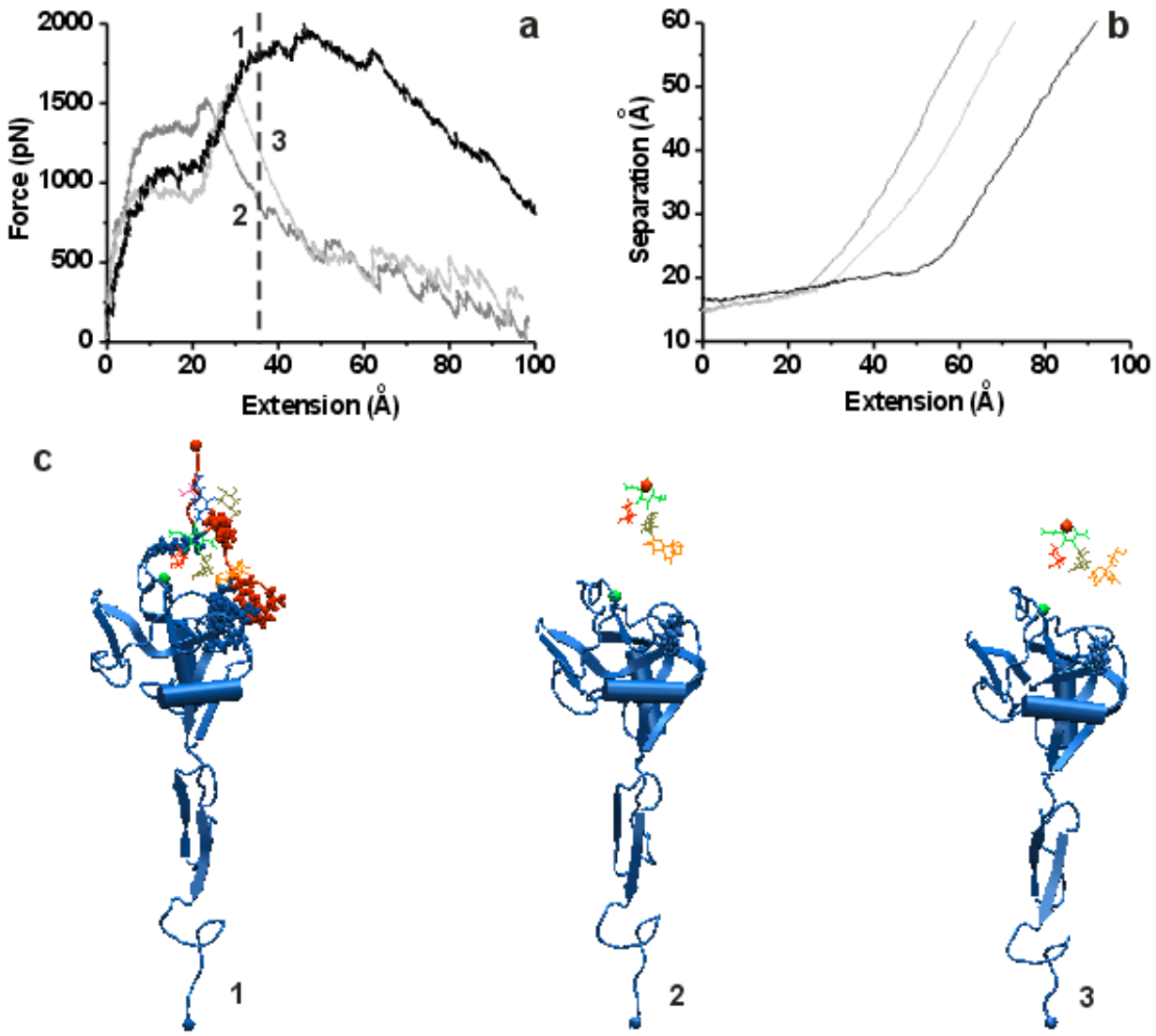

Figure 7 : Dependence of forced dissociation on various selectin-ligand systems at 0.5 Å/ps. (*a*) Force *vs.* extension profiles. (*b*) Corresponding separation evolutions (P-LE/SGP-3: *black*; P-LE/sLe^X: *gray*; E-LE/sLe^X: *light gray*). (*c*) Snapshots at the same extension of 35 Å.

force directions.

Similar results were also found in *cv*-SMD simulation at 0.1 Å/ps with periodic boundary condition and full electrostatic calculations, by comparison with spherical boundary condition and cut-off electrostatic calculations used as the above SMD simulations (*cf.* Fig. 3). The resulted consistency indicated that these two factors did not affect the forced dissociation of P-LE-SGP-3 complex (*data not shown*).

3.5 Dissociation is dependent on the specific structure

Various selectin-ligand complex has the distinct structure of binding pocket, which may affect its biological functionality in different mechanisms [Somers et al (2000)]. To test this hypothesis, *cv*-SMD simulations were compared for three selectin-ligand complexes (P-LE-sLe^X, E-LE-sLe^X, and P-LE-SGP-3) at 0.5 Å/ps (Fig. 7). As compared to the dissociation profile of P-LE-SGP-3 complex (*black lines* in Fig. 7$a-b$, or *gray lines* in Fig. 5$a-b$), the dissociation of P-LE-sLe^X or E-LE-sLe^X complex still exhibited a transition phase with smaller extension of EGF domain (*gray* and *light gray lines* in Fig.

$7a-b$), which corresponded to the destroy of the minor anti-parallel β sheets of EGF domain before FUC dissociated from Ca^{2+} ion (Fig. $7c$). Even then, the P-LE-sLe^X or E-LE-sLe^X complex did not show essential rupture of Lec and EGF domains, since the transition from molecular extension to complex dissociation occurred at the less extension of 23.6 Å for P-LE-sLe^X and 29.9 Å for E-LE-sLe^X complex while it appeared at 48.9 Å for P-LE-SGP-3 complex (Figs. $7a-b$). This was further supported by the smaller D1 and D2 values and reduced backbone RMSD of EGF domain from P-LE-sLe^X or E-LE-sLe^X complex (*data not shown*). Therefore, it is evident that the molecular structure of ligand affected the dissociation of selectin-ligand bonds.

4 Discussions

Selectin-ligand interactions under applied forces have been extensively studied using many experimental technologies [Alon et al (1995); Chen and Springer (1999); Chen and Springer (2001); Marshall et al (2003); Sarangapani et al (2004); Evans et al (2001); Evans et al (2004); Rinko et al (2004); Fritz et al (1998); Hanley et al (2003); Zhang et al (2004); Marshall et al (2005b); Long et al. (2001); Zhu et al. (2002); Huang et al. (2004)]. The underlying mechanism at atomic level, however, has not been well understood yet. The goal of this study is to obtain a basic understanding of the correlation between molecular conformation and binding functionality of selectin-ligand complex. SMD simulations were used to assess the forced dissociation of P-LE-SGP-3, as well as P-LE-sLe^{X}and E-LE-sLe^X complex. The dependence of intramolecular destroy and intermolecular disruption on pulling velocity and forces, and force exertion were quantified. These results contribute to the understandings of how the selectin-ligand interactions are regulated by applied forces at atomic level.

An applicable force field is the pre-requisite for SMD simulations. Based on existing CHARMM22 [MacKerell et al (1998)] and "top/par_all22_sugar.inp" [Kuttel et al (2002)], we built two sets of force field parameters for C2-O-sLe^X and TYS using both analogy and partial optimization approaches, respectively, following the line of building and optimization of CHARMM force field [MacKerell et al (1998); Foloppe and MacKerell (2000)]. *Analogy set* force field was chosen for SMD simulations in the current study. The applicability of newly built-up *Analogy set* force field was further compared with another *Analogy set* force field proposed by Dr. J. Z. Lou from Georgia Institute of Technology (*personal communications*), which was built using the same analogy approach from a different initial carbohydrate model of "CSFF_top/parm.inp" [Kuttel et al (2002)]. The consistency in simulations upon the two sets of force field parameters (*data not shown*) suggested their applicability to investigate forced dissociation of selectin-ligand complex, which may provide a potential approach to assess the interactions between glycosylated and/or sulfated proteins.

Our simulation results showed that the molecular extension of EGF domain and Lec-EGF interface was coupled with forced dissociation of P-LE-SGP-3 complex, which provided the different mechanism as compared to forced dissociation of CD2/CD58 complex [Bayas et al. (2003)]. Even though few direct evidences were found for molecular extension of P-selectin before P-selectin-PSGL-1 dissociation, there exist some structural and functional reasoning implying the potential possibility of P-selectin extension [Lü and Long. (2004)]. On one hand, it is predicted that there are three intradomain disulfide bonds formed from six cysteines in each CR domain of P-selectin [Johnston et al. (1989)]. CR domain is possibly compact and globular with extensive hydrogen-bonding interactions [Chou and Heinrikson. (1997)], suggesting that it is fairly rigid with high resistance to catastrophic unfolding such as titin and fibronectin [Lu et al. (1998); Gao et al. (2002)]. There are also three disulfide bonds in EGF domain with less optimal conformation to stabilize the integrity of the domain [Freedman et al. (1996); Somers et al. (2000)], which turns out that EGF domain may be less rigid with low resistance to applied forces. On the other hand, PSGL-1-expressing leukocytes roll stably on P-selectin immobilized substrate probably due to cell deformation, microvilli tensile, and molecular extension. And PSGL-1- or SGP-3-coated beads roll less but still stably on P-selectin substrate when the effects of cell deformation and microvilli extension were excluded [Chen and Springer. (1999); Yago et al. (2002)]. P-selectin has high elasticity with spring constant of $\sim$ 1.0 pN/nm and as high strain as $\sim$ 500% [Marshall et al. (2005a)]. These observations support the possibility of P-selectin extension during forced dissociation of P-selectin-PSGL-1 interactions. It has been long known that the existence of EGF domain is a prerequisite for selectin binding to its ligand but its

biological functionality is not understood well [Kansas. (1996)]. Our simulations reported here provide a rational of importance of EGF domain to affect the kinetics and mechanics of selectin-ligand interactions.

Although there exist the limitations of short time scale and small system size imposed by limited computer resources, SMD simulations in this study imposed the structural bases of dissociation of P-LE-SGP-3 complex on different velocities and forces. While the distortion of the minor anti-parallel β sheets of EGF domain always appeared before complex dissociation, the sequence of following destroy of the major anti-parallel β sheets of EGF domain and Lec-EGF interface depended strongly on external forces. At high velocity of 1.5 Å/ps (Fig. 5), the partial dissociation of FUC from Ca^{2+} and its nearby residues took place firstly, followed by significant intramolecular destroy and then intermolecular disruption. At intermediate velocities of 1.0 and 0.5 Å/ps (Fig. 5), the intramolecular destroy of the major anti-parallel β sheets of EGF domain and Lec-EGF interface occurred prior to the intermolecular disruption, which evolved further with the evolution of dissociation process. At low velocities of 0.1 and 0.05 Å/ps or all forces of 1500, 1000, and 500 pN (Figs. 3, 5), the intramolecular destroy was almost completed before dissociation initiated. At a *cf*-SMD simulation of 500 pN, the third stable plateau appeared after dissociation of FUC from Ca^{2+} (Fig. 5*c*), resulting from strong binding of R85 with D611 after its separation from Y610. In addition to three sulfated tyrosines (Y605, Y607, and Y610), such acidic residues as D611, D609, and E606 along the peptide of SGP-3 ligand are allowed to bind to basic residue R85 during forced dissociation [Somers et al (2000)], which may form the so-called finger trap during forced dissociation. Such a binding regulates the bond survival at a constant force.

In summary, our SMD simulations of forced dissociations of selectin-ligand complexes presented here provide a mechanism that the intramolecular destroy is coupled to the intermolecular disruption. The molecular extension is mainly determined by the destroy of the two anti-parallel β sheets of EGF domain and of Lec-EGF interface. And the complex dissociation depends on the separation of FUC from Ca^{2+}. Such the conformational changes are modulated by applied velocities and forces, as well as force exertion. More experiments will be needed to test the predictions.

Acknowledgement: We thank Drs. C. Zhu and J. Z. Lou from Georgia Institute of Technology for the useful discussions. This work was supported by NSFC grants 10332060, 30225027, and 10128205, a CAS grant KJCX2-SW-L06 and a NIH grant TW 05774-01. All simulations were performed on the HP-SC45 Sigma-X parallel computer in the Institute of Theoretical Physics and Interdisciplinary Center of Theoretical Studies, Chinese Academy of Sciences.

References

Alon, R.; Hammer, D. A.; Springer, T. A. (1995): Lifetime of the P-selectin: carbohydrate bond and its response to tensile force in hydrodynamic flow. *Nature,* vol. 374, pp. 539-542.

Bayas, M. V.; Schulten, K.; and Leckband, D. (2003): Forced detachment of the CD2-CD58 complex. *Biophys. J.,* vol. 84, pp. 2223-2233.

Bayas, M. V.; Schulten, K.; Leckband, D. (2004): Forced dissociation of the strand dimer interface between C-Cadherin ectodomains. *Mechanics and Chemistry of Biosystems,* vol. 1, pp. 101-111.

Bell, G. I. (1978): Models for the specific adhesion of cells to cells. *Science*, vol. 200, pp. 618-627.

Bernstein, F. C.; Koetzle, T. F.; Williams, G. J.; Meyer, E. F. Jr.; Brice, M. D.; Rodgers, J. R.; Kennard, O.; Shimanouchi, T.; Tasumi, M. (1977): The protein data bank: a computer-based archival file for macromolecular structures. *J. Mol. Biol.,* vol. 112, pp. 535-542.

Brooks, B. R.; Bruccoleri, R. E.; Olafson, B. D.; States, D. J.; Swaminathan, S.; Karplus, M. (1983): CHARMM: A program for macromolecular energy, minimization, and dynamics calculations, *J. Comput. Chem.,* vol. 4, pp. 187-217.

Chen, S.; Springer, T. A. (1999): An automatic braking system that stabilizes leukocyte rolling by an increase in selectin bond number with shear. *J. Cell Biol.,* vol. 144, pp. 185-200.

Chen, S.; Springer, T. A. (2001): Selectin receptor-ligand bonds: formation limited by shear rate and dissociation governed by the Bell model. *Proc. Natl. Acad. Sci. USA*, vol. 98, pp. 950-955.

Chou, K. C.; Heinrikson, R. L. (1997): Prediction of the tertiary structure of the complement control protein

module. *J. Protein Chem.,* vol. 16, pp. 765-773.

Dembo, M.; Tourney, D. C.; Saxman, K.; Hammer, D. (1988): The reaction-limited kinetics of membrane-to-surface adhesion and detachment. *Proc. R. Soc. London*, vol. 234, pp. 55-83.

Evans, E.; Leung, A.; Hammer, D.; Simon, S. (2001): Chemically distinct transition states govern rapid dissociation of single L-selectin bonds under force. *Proc. Natl. Acad. Sci. USA*, vol. 98, pp. 3784-3789.

Evans, E.; Leung, A.; Heinrich, V.; Zhu, C. (2004): Mechanical switching and coupling between two dissociation pathways in a P-selectin adhesion bond. *Proc. Natl. Acad. Sci. USA*, vol. 101, pp. 11281-11286.

Foloppe, N.; MacKerell, Jr. A. D. (2000): All-atom empirical force field for nucleic acids: I. parameter optimization based on small molecule and condensed phase macromolecular target data. *J. Comput. Chem.,* vol. 21, pp. 86-104.

Freedman, S. J.; Sanford, D. G.; Bachovchin, W. W.; Furie, B. C.; Baleja, J. D.; Furie, B. (1996): Structure and function of the epidermal growth factor domain of P-selectin. *Biochemistry*, vol. 35, pp. 13733-13744.

Frisch, M. J.; Trucks, G. W.; Schlegel, H. B.; Scuseria, G. E.; Robb, M. A.; Cheeseman, J. R.; Zakrzewski, V. G.; Montgomery, Jr., J. A.; Stratmann, R. E.; Burant, J. C.; Dapprich, S.; Millam, J. M.; Daniels, A. D.; Kudin, K. N.; Strain, M. C.; Farkas, O.; Tomasi, J.; Barone, V.; Cossi, M.; Cammi, R.; Mennucci, B.; Pomelli, C.; Adamo, C.; Clifford, S.; Ochterski, J.; Petersson, G. A.; Ayala, P. Y.; Cui, Q.; Morokuma, K.; Salvador, P.; Dannenberg, J. J.; Malick, D. K.; Rabuck, A. D.; Raghavachari, K.; Foresman, J. B.; Cioslowski, J.; Ortiz, J. V.; Baboul, A. G.; Stefanov, B. B.; Liu, G.; Liashenko, A.; Piskorz, P.; Komaromi, I.; Gomperts, R.; Martin, R. L.; Fox, D. J.; Keith, T.; Al-Laham, M. A.; Peng, C. Y.; Nanayakkara, A.; Challacombe, M.; Gill, P. M. W.; Johnson, B.; Chen, W.; Wong, M. W.; Andres, J. L.; Gonzalez, C.; Head-Gordon, M.; Replogle, E. S.; Pople, J. A. (2001): GAUSSIAN98, Revision A.1*x*; Gaussian, Inc.: Pittsburgh, PA.

Fritz, J.; Katopodis, A. G.; Kolbinger, F.; Anselmetti, D. (1998): Force-mediated kinetics of single P-selectin/ligand complexes observed by atomic force microscopy. *Proc. Natl. Acad. Sci. USA*, vol. 95, pp. 12283-12288.

Gao, M.; Craig, D.; Vogel, V.; Schulten, K. (2002): Identifying unfolding intermediates of FN-III_{10} by steered molecular dynamics. *J. Mol. Biol.*, vol. 323, pp. 939-950.

Hanley, W.; McCarty, O.; Jadhav, S.; Tseng, Y.; Wirtz, D.; Konstantopoulos, K. (2003): Single molecule characterization of P-selectin/ligand binding. *J. Biol. Chem.,* vol. 278, pp. 10556-10561.

Huang, J.; Chen, J.; Chesla, S. E.; Yago, T.; Mehta, P.; McEver, R. P.; Zhu, C., and Long, M. (2004): Quantifying the effects of molecular orientation and length on two-dimensional receptor-ligand binding kinetics. *J. Biol. Chem.*, vol. 279, pp. 44915–44923.

Humphrey, W.; Dalke, A.; Schulten, K. (1996): VMD-visual molecular dynamics. *J. Mol. Graph.*, vol. 14, pp. 33-38.

Isralewitz, B.; Gao, M.; Schulten, K. (2001): Steered molecular dynamics and mechanical functions of proteins. *Curr. Opin. Struct. Biol.*, vol. 11, pp. 224-230.

Izrailev, S.; Stepaniants, S.; Balsera, M.; Oono, Y.; Schulten, K. (1997): Molecular dynamics study of unbinding of the avidin-biotin complex. *Biophys. J.*, vol. 72, pp. 1568-1581.

Johnston, G. I.; Cook, R. G.; McEver, R. P. (1989): Cloning of GMP-140, a granule membrane protein of platelets and endothelium: sequence similarity to proteins involved in cell adhesion and inflammation. *Cell,* vol. 56(6), pp. 1033-1044.

Kale, L. V.; Skeel, R. D.; Bhandarkar, M.; Brunner, R.; Gursey, A.; Krawetz, N.; Philips, J.; Shinazaki, A.; Varadarajan, K.; Schulten, K. (1999): NAMD2: greater scalability for parallel molecular dynamics. *J. Comput. Phys.*, vol. 151, pp. 283-312.

Kansas, G. S. (1996): Selectins and their ligands: current concepts and controversies. *Blood*, vol. 88, pp. 3259-3287.

Kirschner, K. N.; Woods, R. J. (2001): Solvent interactions determine carbohydrate conformation. *Proc. Natl. Acad. Sci. USA,* vol. 98, pp. 10541-10545.

Kuttel, M.; Brady, J. W.; Naidoo, K. J. (2002): Carbohydrate solution simulations: producing a force field with experimentally consistent primary alcohol rotational frequencies and populations. *J. Comput. Chem.,* vol. 23, pp. 1236-1243.

Lawrence, M. B.; Springer, T. A. (1991): Leukocytes

roll on a selectin at physiologic flow rates: distinction from and prerequisite for adhesion through integrins. *Cell*, vol. 65, pp. 859-873.

Leppänen, A.; **Mehta, P.; Ouyang, Y. B.; Ju, T. Z.; Helin, J.; Moore, K. L.; Die**, I. V.; **Canfield, W. M.; McEver**, R. P.; **Cummings, R. D.** (1999): Novel glycosulfopeptide binds to P-selectin and inhibits leukocyte adhesion to P-selectin. *J. Biol. Chem.,* vol. 274, pp. 24838-24848.

Leppänen, A.; Yago, T.; Otto, V. I.; McEver, R. P.; Cummings, R. D. (2003): Model glycosulfopeptides from P-selectin glycoprotein ligand-1 require tyrosine sulfation and a core-2-branched O-glycan to bind to L-selectin. *J. Biol. Chem.,* vol. 278, pp. 26391-26400.

Ley, K.; Gaehtgens, P.; Fennie, C.; Singer, M. S.; Lasky, L. A.; Rosen, S. D. (1991): Lectin-like Cell Adhesion Molecule 1 mediates leukocyte rolling in mesenteric venules in vivo. *Blood*, vol. 77, pp. 2553-2555.

Li, F.; Erickson, H. P.; James, J. A.; Moore, K. L.; Cummings, R. D.; McEver, R. P. (1996): Visualization of P-selectin glycoprotein ligand-1 as a highly extended molecule and mapping of protein epitopes for monoclonal antibodies. *J. Biol. Chem.,* vol. 271, pp. 6342-6348.

Long, M.; Zhao, H.; Huang, K.-S.; and Zhu, C. (2001): Kinetic measurements of cell surface E-selectin/carbohydrate ligand interactions. *Ann. Biomed. Engi.*, vol. 29, pp. 935-946.

Lu, H.; Isralewitz, B.; Karmmer, A.; Vogel, V.; Schulten, K. (1998): Unfolding of titin Immunoglobulin domains by steered molecular dynamics simulation, *Biophys. J.*, vol. 75, pp. 662-671.

Lü, S. Q.; and Long, M. (2004): Forced extension of P-selectin construct using steered molecular dynamics. *Chinese Science Bulletin*, vol. 49, pp. 10-17.

MacKerell, Jr. A. D.; Bashford, D.; Bellot, M.; Dunbrack, Jr. R. L.; Evansec, J.; Field, M. J.; Fisher, S.; Gao, J.; Guo, H.; Ha, S.; Joseph, D.; Kuchnir, L.; Kuczera, K.; Lau, F. T. K.; Mattos, C.; Michnick, S.; Ngo, T.; Nguyen, D. T.; Prodhom, B.; Reiher, I. W. E.; Roux, B.; Schlenkrich, M.; Smith, J.; Stote, R.; Straub, J.; Watanabe, M.; Wiorkiewicz-Kuczera, J.; Yin, D.; Karplus, M. (1998): All-hydrogen empirical potential for molecular modeling and dynamics studies of proteins using the CHARMM22 force field. *J. Phys. Chem. B.*,vol. 102, pp. 3586–3616.

Marshall, B. T.; Long, M.; Piper, J. W.; Yago, T.; McEver, R. P.; Zhu, C. (2003): Direct observation of catch bonds. *Nature*, vol. 423, pp. 190-193.

Marshall B. T.; Sarangapani K. K.; Wu J. H.; Lawrence M.; McEver R. P.; Zhu C. (2005a): Measuring molecular elasticity by atomic force microscope cantilever fluctuations. *Biophys. J.*, vol. 90, pp. 681-692.

Marshall, B. T.; Sarangapani, K. K.; Lou, J. Z.; McEver, R. P.; Zhu, C. (2005b): Force history dependence of receptor-ligand dissociation. *Biophys. J.*, vol. 88, pp. 1458-1466.

Marszalek, P. E.; Lu, H.; Li, H.; Carrion-Vazquez, N.; Oberhauser, A. F.; Schulten, K.; Fernandez, J. M. (1999): Mechanical unfolding intermediates in titin modules. *Nature,* vol. 402, pp. 100-103.

McEver, R. P. (2001): Adhesive interactions of leukocytes, platelets, and the vessel wall during hemostasis and inflammation. *Thromb. Haemost.,* vol. 86, pp. 746-756.

McEver, R. P. (2002): Selectins: lectins that initiate cell adhesion under flow. *Curr. Opin. Cell. Biol.,* vol. 14, pp. 581-586.

Merkel, R.; Nassoy, P.; Leung, A.; Ritchie, K.; Evans, E. (1999): Energy landscapes of receptor-ligand bonds explored with dynamic force spectroscopy. *Nature*, vol. 397, pp. 50-53.

Moore, K. L.; Stults, N. L.; Diaz, S.; Smith, D. F.; Cummings, R. D.; Varki, A.; McEver, R. P. (1992): Identification of a specific glycoprotein ligand for P-selectin (CD62) on myeloid cells. *J. Cell. Biol.*, vol. 118, pp. 445-456.

Ramachandran, V.; Nollert, M. U.; Qiu, H. Y.; Liu, W. J.; Cummings, R. D.; Zhu, C.; McEver, R. P. (1999): Tyrosine replacement in P-selectin glycoprotein ligand-1 affects distinct kinetic and mechanical properties of bonds with P- and L-selectin. *Proc. Natl. Acad. Sci. USA,* vol. 96, pp. 13771-13776.

Rinko, L. J.; Lawrence, M. B.; Guilford, W. H. (2004): The molecular mechanics of P- and L-selectin Lectin domains binding to PSGL-1. *Biophys. J.,* vol. 86, pp. 544-554.

Sarangapani, K. K.; Yago, T.; Klopocki, A. G.; Lawrence, M. B.; Fieger, C. B.; Rosen, S. D.; McEver, R. P.; Zhu, C. (2004): Low force decelerates L-selectin

dissociation from P-selectin glycoprotein ligand-1 and endoglycan. *J. Biol. Chem.*, vol. 279, pp. 2291-2298.

Somers, W. S.; Tang, J.; Shaw, G. D.; Camphausen, R. T. (2000): Insight into the molecular basis of leukocyte tethering and rolling revealed by structures of P- and E-selectin bound to sLe^X and PSGL-1. *Cell,* vol. 103, pp. 467-479.

Springer, T. A. (1990): Adhesion receptors of the immune system. *Nature,* vol. 346, pp. 425-434.

Springer, T. A. (1994): Traffic signals for lymphocyte recirculation and leukocyte emigration: The multi-step paradigm. *Cell,* vol. 76, pp. 301-314.

Ushiyama, S.; Laue, T. M.; Moore, K. L.; Erickson, H. P.; McEver, R. P. (1993): Structural and functional characterization of monomeric soluble P- selectin and comparison with membrane P-selectin. *J. Biol. Chem.*, vol. 268, pp. 15229-15237.

Vestweber, D.; Blanks, J. E. (1999): Mechanisms that regulate the function of the selectins and their ligands. *Physiol. Rev.*, vol. 79, pp. 181-213.

Yago, T.; Leppänen, A.; Qiu, H. Y.; Marcus, W. D.; Nollert, M. U.; Zhu, C.; Cummings, R. D.; McEver, R. P. (2002): Distinct molecular and cellular contributions to stabilizing selectin-mediated rolling under flow. *J. Cell Biol.*, vol. 158, pp.787-799.

Zhang, X. H.; Bogorin, D. F.; Moy, V. T. (2004): Molecular basis of the dynamic strength of the sialyl Lewis X-selectin interaction. *ChemPhysChem,* vol. 5, pp. 175-182.

Zhu, C; Long, M.; Chesla, S. E.; and Bongrand, P. (2002): Measuring receptor/ligand interaction at the single bond level: Experimental and interpretive issues. *Ann. Biomed. Engi.*, vol. 30, pp. 305-314.